Mon. Not. R. Astron. Soc. **280,** 1027–1034 (1996)

New H I absorption measurements towards six pulsars

T. P. Saravanan,[1] A. A. Deshpande,[1] W. Wilson,[2] E. Davies,[2] P. M. McCulloch[3] and D. McConnell[4]

[1]*Raman Research Institute, Bangalore 560 080, India*
[2]*Australia Telescope National Facility, CSIRO, PO Box 76, Epping, NSW 2121, Australia*
[3]*Physics Department, University of Tasmania, GPO Box 252C, Hobart, TAS 7001, Australia*
[4]*Australia Telescope National Facility, Locked Bag 194, Narrabri, NSW 2390, Australia*

Accepted 1995 December 14. Received 1995 December 11; in original form 1995 August 4

ABSTRACT

New H I absorption measurements made towards six pulsars are presented. Kinematic distance limits are derived for five of them. Mean line-of-sight electron densities are estimated using the dispersion measures of the pulsars. Temperatures are derived for the cold absorbing H I clouds from the amount of absorption seen in the observed pulsar spectra.

Key words: pulsars: individual: J0908 – 4913 – pulsars: individual: J1326 – 5859 – pulsars: individual: J1740 – 3015 – pulsars: individual: J1745 – 3040 – pulsars: individual: J1824 – 1945 – ISM: general.

1 INTRODUCTION

H I absorption spectra observed against pulsars give useful constraints on distances to the pulsars. Such measurements also help us to probe the electron density distribution in the Galaxy and also the physical conditions in the cold absorbing H I clouds. Unlike the absorptions measured against *continuous* sources, the absorption spectra against pulsars give the 'true' absorption as one need not depend on nearby sight lines to estimate the *off-source* spectrum.

To determine distance limits to a pulsar, the H I absorption spectrum seen against the pulsar is interpreted using the relation between the radial velocity and distance, derived from a model for the rotation of the Galaxy. The presence of an absorption feature gives a lower limit for the distance to the pulsar. Wherever the observed H I emission is in excess of 35 K, cold absorbing H I clouds are expected to be reasonably well distributed along the sight lines (Radhakrishnan et al. 1972; Payne, Salpeter & Terzian 1983). An absence of absorption features in the velocity range where the antenna temperature in the H I emission spectrum is in excess of ~35 K can therefore be used to obtain upper limits to the distance of the pulsar (Frail & Weisberg 1990).

Once the distance to a pulsar is known from the kinematic interpretations of the H I absorption spectrum (or from association with other astronomical objects or from parallax measurements), the dispersion measure (DM) of the pulsar can be used to constrain the model of electron density distribution in the Galaxy (e.g. Taylor & Cordes 1993). A reliable model for the electron density distribution in the Galaxy is useful to estimate distances to pulsars using their DMs in cases where independent distances are not available or possible.

So far, H I observations have been made towards ~75 pulsars (see Frail & Weisberg 1990). In this paper, we present new measurements of the H I absorption towards six southern pulsars. Since there are considerably fewer southern pulsars with known H I distance estimates, even these few new estimates should offer useful additional constraints for the models of the electron density distribution

The details of our observations are presented in Section 2 and the data analysis is discussed in Section 3. In Section 4 we present the results of these observations and our interpretation of the absorption spectra with a view to obtaining distance limits. Using the derived distances, we estimate the average electron densities along the sight lines to these pulsars. We also estimate approximate spin temperatures of the H I clouds from the optical depths of absorptions observed.

2 OBSERVATIONS

The observations were made during 1994 February 1–2 using the Parkes Radiotelescope of the Australia Telescope National Facility. Measurements were made using a dual linear polarization feed and a dual channel receiver at 1420 MHz. An intermediate frequency (IF) bandwidth of 4 MHz

was used with a 2×512 channel autocorrelator spectrometer giving a frequency resolution of 7.8 kHz (the corresponding velocity resolution being 1.6 km s^{-1}).

The data were acquired from the spectrometer in a specially designed *gating* mode. In this mode the spectra (obtained by Fourier transforming the autocorrelation function measured over the pre-specified integration interval) are averaged synchronously with the pulsar period divided into a chosen number of phase bins (say, N_b) to obtain integrated spectra corresponding to individual (pulsar) phase bins. The number of bins (8, 16 or 32) is chosen such that the bin width is as small as possible (but ≥ 10 ms), so as to sample the pulsar signal with a maximum time resolution. The bin widths can be chosen in multiples of 1 μs. Any residual differences (part of 1 μs) between bin width times the number of bins and the pulsar period is accommodated in the first bin. Thus the first bin has slightly different width (by an amount N_b μs in the worst case) than other bins. Care is taken to minimize the number of bins receiving *on-pulse* spectra (so as to maximize the signal-to-noise ratio) and to avoid the first bin. This was done by monitoring the total-power output corresponding to the 4-MHz band during observations using a digital integrating cathode-ray oscilloscope. The first bin which corresponds to the *off-pulse* region is excluded from the data analysis. In all cases the *on-pulse* region of the pulse profiles occupies one or two bins.

The acquired spectra corresponding to different bins are integrated on-line separately for each of the 20–30 s intervals and the integrated spectra in each of these intervals are recorded. The pulse arrival time differences owing to the differential dispersion across the bandwidth of 4 MHz would be only a few milliseconds, even for a pulsar with a DM of ~ 300 cm^{-3} pc. In most of the cases this delay difference across the band is considerably less than the bin width used (≥ 10 ms), ensuring that the on-pulse bins are not noticeably staggered across the spectrum.

Since the correlator is used with an automatic gain control (AGC) before the sampler, no total power information is readily available from the spectrum itself. Hence the total power was recorded along with the spectrum. Also, a CW signal was injected before the AGC for calibration purposes, but is not used during the present analysis as the total power recorded provided a sufficiently accurate calibration.

The total time for which each pulsar was observed and the number of bins used over the pulsar period are given in Table 1.

3 DATA ANALYSIS

The recorded data consist of spectra averaged (for 20–30 s) in each of the phase bins across the pulsar period. Such sets are further combined to obtain block averages over 15 min. Every combined spectrum is calibrated using the recorded total power information, and then combined further. The band-shape model is derived for both polarization channels from the H I spectrum in the direction of PSR 0743 − 53. This spectrum has only one sharp feature, which is masked off before fitting for the band shape with polynomials and sinusoids. The fit is seen to model the band shape resonably well (with 1 per cent) over the channel range 90–425. This model is used to provide a relative gain calibration across the spectrum. About 100 channels on both ends of the spectrum are omitted from further processing, as these regions are affected by relatively higher noise and poor calibration of the band shape. The total power in the selected channels is used to determine the average pulse profile. All spectra are corrected by dividing by the model to give equal weights to all selected channels, thus increasing the effective bandwidth and increasing the signal-to-noise ratio in the pulse profile.

Table 1. Observation parameters.

Pulsar	integration time (min.)	bins
PSR 0905−51	330	16
PSR 0906−49	295	8
PSR 1323−58	225	32
PSR 1737−30	237	32
PSR 1742−30	173	32
PSR 1821−19	377	16

The bins containing the pulse are identified from the pulse profile. The spectra corresponding to the *on-pulse* bins and the *off-pulse* bins are combined separately to construct the *on* and *off* spectra, respectively. (The *on* spectra are weighted by the pulse contribution in different bins, in order to optimize the signal-to-noise ratio.) The absorption spectrum is simply the difference between the *on* and *off* spectra. The noise in the *on* or *off* spectrum in turn is inversely proportional to the square root of the equivalent number of bins used to obtain the corresponding spectra. As the pulse only occupies a small fraction of a period, the noise in the absorption spectrum is dominated by the noise contribution from the *on* spectrum. The absorption spectra thus obtained are smoothed using a two-channel-wide smoothing window in order to improve detectability of relatively weak absorption features.

The emission spectra are calibrated with respect to their baseline values which contain contributions from continuum emission in the observed direction and the receiver noise temperature. The continuum temperatures are taken from surveys (Mathewson, Healy & Rome 1962; Altenoff et al. 1970; Sinclair & Kerr 1971). The receiver temperature is calibrated using observations towards a continuum source PKS 1934 − 638 (from a previous session in 1992 November) and is estimated to be ~ 37 K.

3.1 A new procedure for estimating baselines in absorption spectra

Reliable estimation and removal of residual baselines in the absorption spectra is crucial in identifying weak absorption features. The baselines are not flat even after proper calibration of the band shape, particularly if the diffractive scintillations of the pulsar signal are not averaged out suffiiently over the integration time. This is important when the decorrelation bandwidths are smaller than or of the order of the width of the band being observed.

A common problem in baseline fitting is that of identifying the line features so as to exclude these regions while fitting a suitable baseline model to the rest of the spectrum. If one does not exclude all of the line features, the fitting procedure will fit for the feature too and remove its contribution as a part of the baseline variation. On the other

hand if one is overcautious in specifying the regions for fitting, say, by leaving out the region in the absorption spectrum in the velocity range where the emission spectrum has line emission present, the fit is poorly constrained. In order to overcome this problem, a following iterative procedure is considered wherein the region to be fitted is selected in an adaptive way.

In the first iteration, the fitting routine is applied over the entire absorption spectrum, i.e. without masking out any part of it. Sinusoidal functions with periods down to one-tenth of the total spectral span are used to fit the baseline of the spectrum. The regions where the spectrum deviates on the negative side from the fit by more than three times the expected rms in the corresponding channel are identified as regions that may correspond to an absorption feature. Each such region, as well as regions of similar width on either side of it, are excluded from the spectrum for the next iteration of baseline fitting. The fitting routine is applied now to the rest of the spectrum: the deviations from the model are assessed again across the entire spectrum and the procedure is repeated until the fit stabilizes. It is observed that the model for the baseline stabilized in a few iterations and that the procedure does not produce any obvious spurious features. The expected rms noise in each channel of the spectrum is estimated by including the contribution from the H I emission features to the system temperatutre in the different channels (Deshpande et al. 1992). For this purpose, the corresponding H I emission profile is used directly to describe the varying antenna temperature across the spectrum.

4 RESULTS

We have used the galactic rotation model of Fich, Blitz & Stark (1989) to interpret the velocities corresponding to the absorption in terms of distances to the absorbing clouds. This model uses a flat rotation curve with the standard Galactic rotation parameters: Θ_0 (rotation speed) = 220 km s^{-1} and R_0 (distance to the centre of the Galaxy) = 8.5 kpc.

The estimates of the spin temperature mentioned in the following subsections should be viewed with some caution. The reliability of these estimates is affected by the following factors. (1) There is a serious difficulty in estimating the fraction of the observed H I column density (inferred from the observed H I emission) that is associated with the regions contributing to a particular absorption feature in the pulsar spectra. This difficulty arises for various reasons. First, the observed column density is an average over the telescope beamwidth. Secondly, the dominant contribution to the observed H I emission often comes from the warmer components. Thirdly, the observed emission includes also the contribution from H I beyond the location of the pulsar, while the observed absorption is only due to the matter in the foreground of the pulsar. It may be possible to overcome the latter problems in directions where adequate distance resolution along the sight line can be achieved. In general, however, this difficulty results in an overestimation of the column density associated with the observed absorption, and hence in a similar bias in the estimation of the spin temperatures. (2) If the observed absorption is contributed by a number of H I clouds with varying physical conditions along the sight line, then the spin temperaure estimated in a simple manner corresponds to a weighted harmonic mean (along the sight line) of the spin temperatures. This leads to, in general, an underestimation of the 'true' spin temperature.

4.1 PSR 0905 − 51

PSR 0905 − 51 has a 253-ms period (Siegman, Manchester & Durdin 1993) and an average flux density of 9 mJy at 1400 MHz (Wu et al. 1993). Though this pulsar has a DM of 104 cm^{-3} pc (Newton, Manchester & Cooke 1981) the H I spectrum towards this pulsar presented in Fig. 1(a) shows no significant absorption feature. All fluctuations lie within $\sim 2\sigma$. We do not derive any distance limits to this pulsar owing to the lack of any significant absorption.

4.2 PSR 0906 − 49

PSR 0906 − 49 has a short period (103 ms) with strong interpulse and a high degree of linear polarization (D'Amico et al. 1988; Wu et al. 1993). It has an average flux density of 16 mJy and a DM of 179 cm^{-3} pc (Johnston et al. 1992). As seen in Fig. 1(b), there is strong absorption in the velocity range ~ -10 to $+15$ km s^{-1}. The farthest feature in this range, at the point of deepest absorption, corresponds to a distance of ~ 3 kpc. The spectra presented in Fig. 1(b) do not include the data from the interpulse region incurring only a small penalty in the signal-to-noise ratio for the absorption profile. There is some emission and absorption at negative velocities beyond those implied by the rotation curve, which can be understood as being caused by random velocities of local clouds. A relatively weak but significant ($\sim 3\sigma$) feature can be discerned at 50 km s^{-1}; this would correspond to a distance of ~ 7 kpc. Although chance excursions of this level are not uncommon owing to the increased random noise in the regions of higher system temperatures (for example, the positive excursions in the absorption spectra for PSRs 1730 − 30 and 1743 − 30), the apparent width of this feature at 50 km s^{-1} argues that it is more likely to be 'real'. Since there is strong emission at velocities just beyond this feature with no corresponding absorption, this distance is likely to be the distance to the pulsar itself. Accounting for possible random motions of the order of 7 km s^{-1}, the estimated distance to this pulsar is ~ 6.3–7.7 kpc. This is closer to the upper limit on the distance derived from recent measurements by Koribalski et al. (1995). The absorption profile presented by them does not show the 50 km s^{-1} feature, and the detection of it from our observations considerably narrows down the distance estimates to the pulsar. (We would like to mention in passing that the measurements by Koribalski et al. 1995 and by us were made with only a few days gap between them, and using the same equipment. We have taken extra care to assess the reliability of this feature in our absorption spectrum and we conclude that this feature is not an artefact.) This constrains the average electron density in this line of sight (to the pulsar) to a value 0.023 cm^{-3} $< \langle n_e \rangle <$ 0.028 cm^{-3}.

A maximum optical depth of 2–3 in the velocity range of 0–10 km s^{-1} implies spin temperatures in the order of 30–45 K.

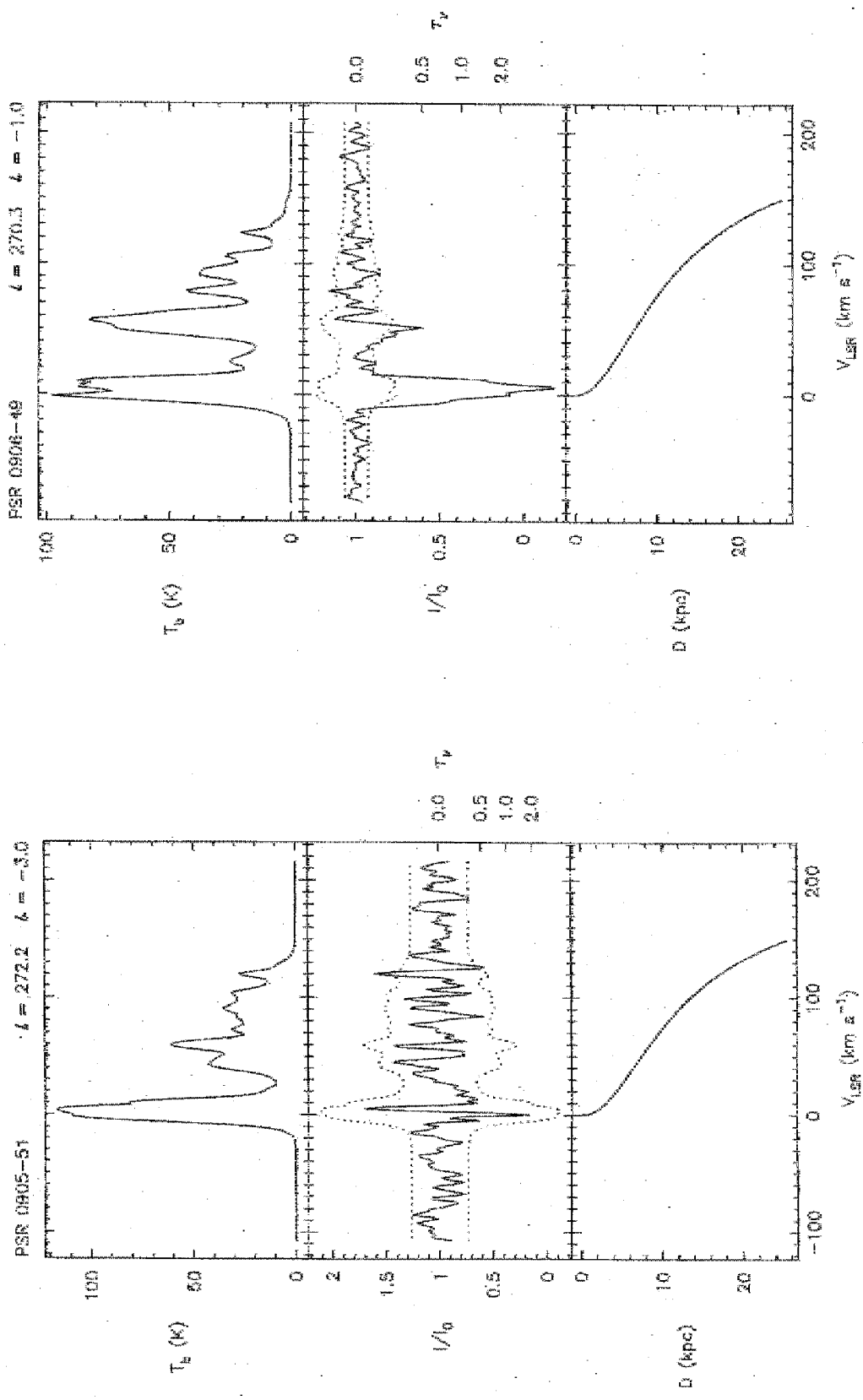

Figure 1. The emission spectrum (top panel), the normalized absorption spectrum (middle panel) and the velocity–distance relation (bottom panel) towards (a) PSR 0905 − 51; (b) PSR 0906 − 49; (c) PSR 1323 − 58; (d) PSR 1737 − 30; (e) PSR 1742 − 30; (f) PSR 1821 − 19. The error envelopes corresponding to $\pm 2\sigma$ error bars are indicated (by dotted lines) along with the absorption profiles to help assessment of the significance of various absorption features. The error estimation may have 10 per cent uncertainty in the worst case. Note that the absorption spectra have been smoothed with a two-channel-wide smoothing function.

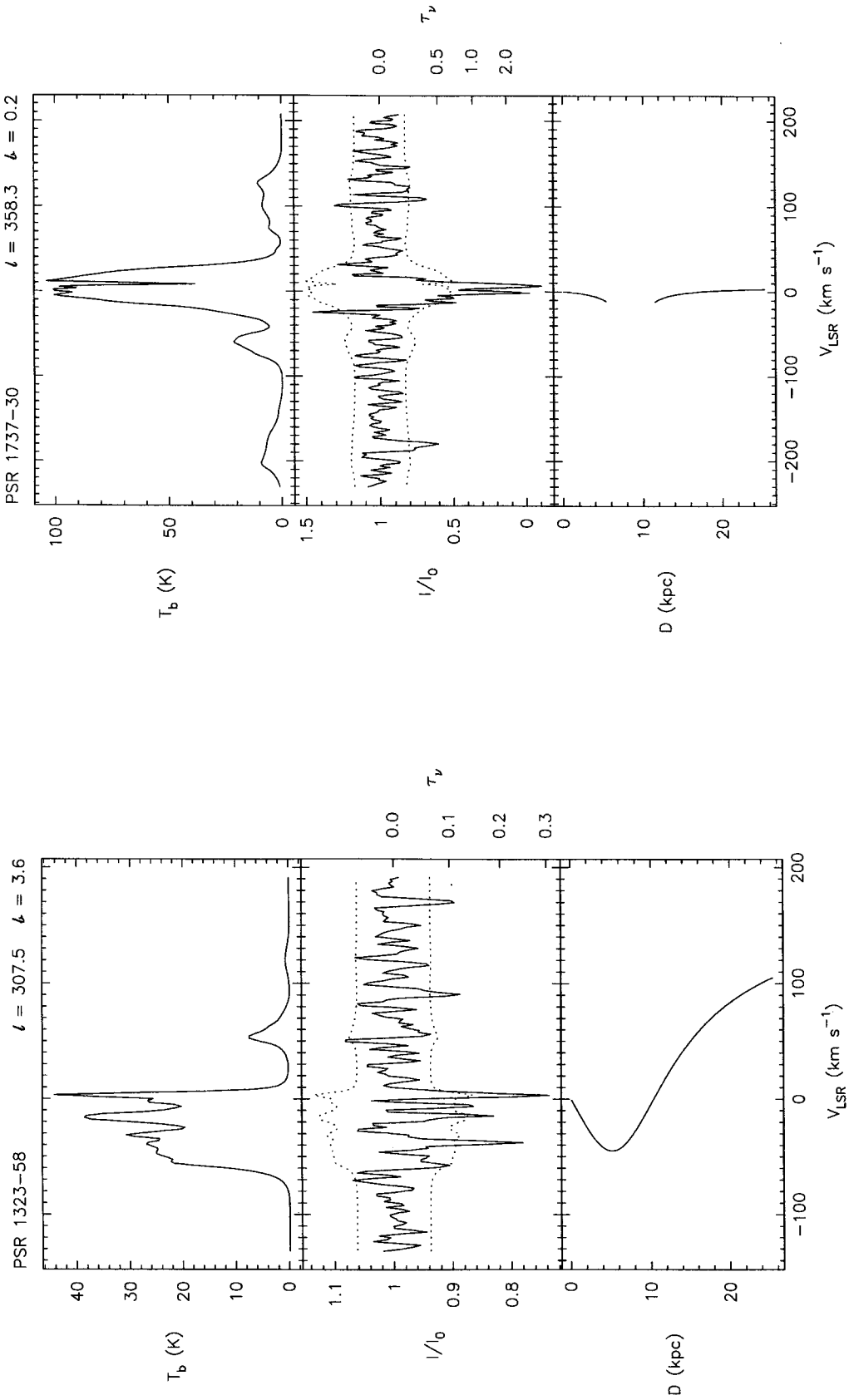

Figure 1 – *continued*

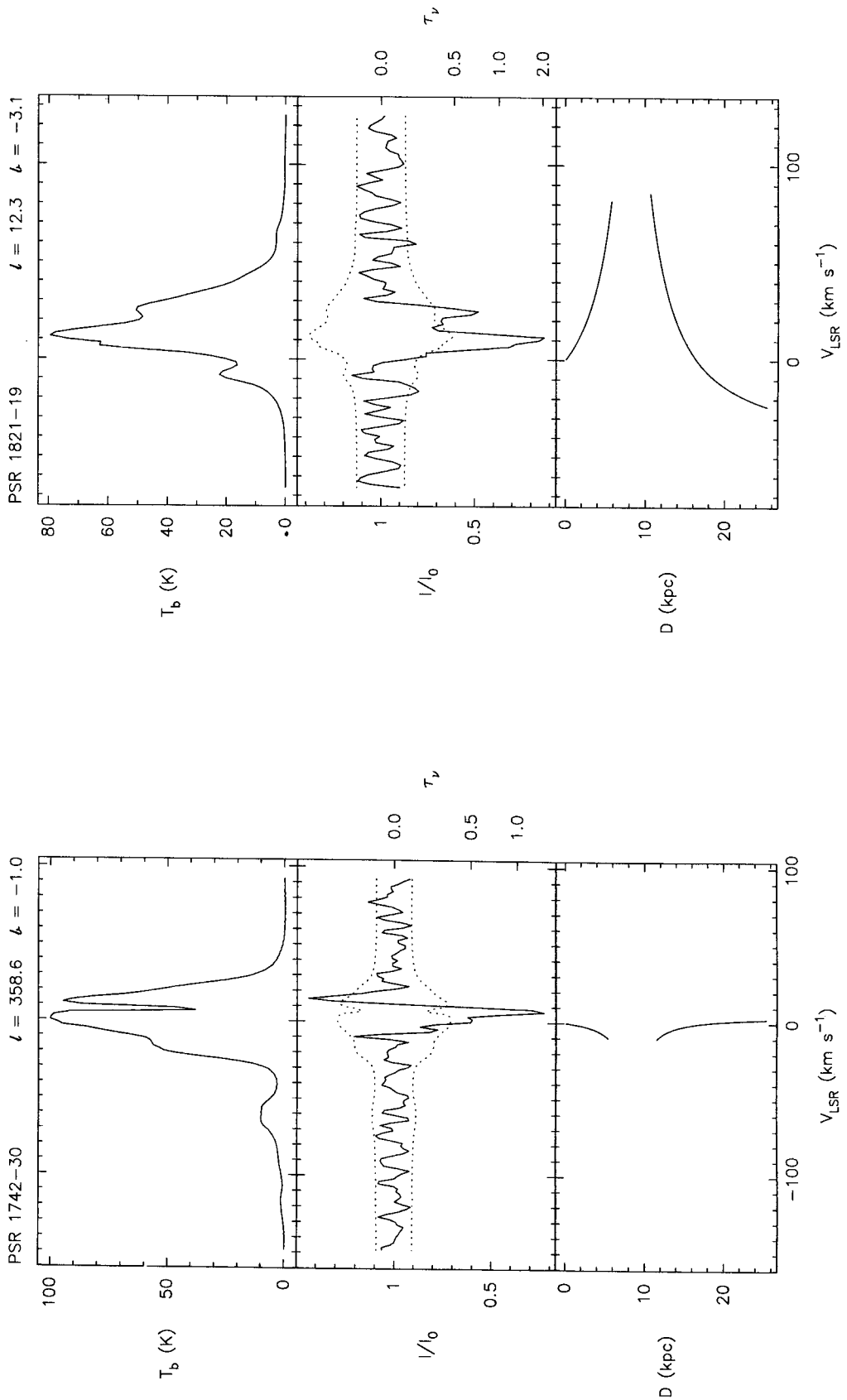

Figure 1 – *continued*

4.3 PSR 1323 − 58

This has a period of 478 ms (Newton, Manchester & Cooke 1981), an average flux density of 10 mJy at 1400 MHz (Wu et al. 1993) and a high DM of 283 cm^{-3} pc (Costa, McCulloch & Hamilton 1991). The H I absorption profile towards this pulsar (Fig. 1c) shows weak narrow absorption features at ~ -40, -16, -8 and 2 km s^{-1}. In this direction the velocity–distance relation is double-valued for negative velocities. To get good lower limits on the distance to the pulsar we must use the left-most feature along with the upper portion of the velocity–distance curve, or the right-most feature along with the lower portion of the velocity–distance curve. The left-most feature (~ -38 km s^{-1}) along with the upper portion of the curve, with 7 km s^{-1} correction for random velocities, towards the nearer side (since we are deriving the lower limit), gives a distance of 3 kpc as the lower limit. The right-most feature within the 7 km s^{-1} random velocity falls in the upper portion of the curve so that it is not possible to interpret it as due to H I at 10 kpc, as it could be caused by local H I corresponding to the upper portion of the curve. Close to the tangent point the emission falls off steeply and the absorption profile is too noisy to ascertain whether or not the absorption extends up to the tangent point. Considering all this, the confident lower limit one can ascribe to this pulsar is $\sim$3 kpc. This limits the mean electron density in this direction to the pulsar to a value of less than 0.094 cm^{-3}.

Since the maximum optical depth is of the order of 0.35, with corresponding emission brightness temperatures of the order of 40 K, the spin temperatures of the absorbing clouds should be $\sim$110 K.

4.4 PSR 1737 − 30

PSR 1737 − 30 discovered by Clifton et al. (1992) is a 600-ms pulsar (S_{1400} = 6 mJy) (Lorimer et al. 1995). It has a DM of 153 cm^{-3} pc and lies close to the direction of the Galactic Centre (l = 358°). The H I absorption profile towards this pulsar is shown in Fig. 1(d). As seen in the figure, even in the range of velocities where a flat rotation model is applicable it has a steep slope and is therefore not useful for interpretation of distance from velocity.

The weak emission feature centred at ~ -60 km s^{-1} corresponds to the '3-kpc expanding arm'. Absorption measurements towards nearby lines of sight, e.g. Sgr A (Kerr & Vallak 1967) and 1739 − 298 (Dickey et al. 1983), show strong absorption against the '3-kpc arm', although the emission is not strong. Assuming that the 3-kpc arm has enough absorbing cold H I, the lack of the absorption feature at the corresponding velocity gives an upper limit to the distance of the pulsar as 5.5 kpc. From this we can infer a lower limit for the average electron density as 0.027 cm^{-3}.

As the optical depth reaches a maximum value of $\sim$2.0, with emission brightness temperatures of $\sim$100 K in the same velocity range, one can infer spin temperatures of 50 K for absorbing clouds in this direction.

4.5 PSR 1742 − 30

PSR 1742 − 30 is a 367-ms pulsar with 14-mJy average flux density at 1400 MHz, with a DM of 89 cm^{-3} pc (Hamilton & Lyne 1988; Siegman et al. 1993; Lorimer et al. 1995). This pulsar, like PSR 1737 − 30, is close to the direction of the Galactic Centre and, in this case too, the velocity–distance model breaks down and fails to be useful. In the spectra presented in Fig. 1(e) the emission feature corresponding to the 3-kpc expanding arm (-60 km s^{-1}) is clearly visible in emission but not in absorption. So using the same interpretation as for the previous pulsar, an upper distance limit of 5.5 kpc can be inferred. The average electron density along this line of sight is more than 0.016 cm^{-3}.

Since the optical depth reaches a maximum value of $\sim$1.0 and the corresponding emission brightness temperature is of the order of 100 K, one can infer spin temperatures of $\sim$100 K for cold absorbing clouds in this direction.

4.6 PSR 1821 − 19

This pulsar has a period of 189 ms, average flux density of 9 mJy at 1400 MHz, and a DM of 224 cm^{-3} pc (Hamilton & Lyne 1988; Siegman et al. 1993; Lorimer et al. 1995). The H I absorption presented in Fig. 1(f) is strong in the range $\sim$0–30 km s^{-1} and there is no absorption elsewhere. The lower limit to the distance will be the one corresponding to the 27 km s^{-1} feature, interpreted with the upper portion of the rotation curve. This, along with an allowance for 7 km s^{-1} for random motions, gives a lower limit of 2 kpc. It is difficult to derive an upper limit as there is not much emission at other velocities, and the lack of absorption might just be because of a lack of cold H I to absorb the pulsar radiation. The distance of 2 kpc implies that the average electron density is less than 0.112 cm^{-3}.

The maximum optical depth is of the order of 2, with a corresponding emission brightness temperature of $\sim$80 K implying a spin temperature of $\sim$40 K in this direction for the absorbing clouds.

5 CONCLUSIONS

All distance limits obtained are listed in Table 2 along with the derived average electron density and the electron

Table 2. Observed pulsars, their parameters and derived H I distances.

PSR name (B1950)	PSR name (J2000)	l (long.) (°)	b (latt.) (°)	S_{1400} (mJy)	Period (msec)	DM (cm^{-3} pc)	DM distance (kpc)	HI distance (kpc)	$\langle n_e \rangle$ derived (cm^{-3})	$\langle n_e \rangle$ model (cm^{-3})
0905−51	0907-5157	272.2	−3.0	9	253.6	104	2.6	—		0.039
0906−49	0908-4913	270.3	−1.0	16	106.8	179	6.6	7.0±0.7	0.026±0.003	0.027
1323−58	1326-5859	307.5	+3.6	10	478.0	283	9.3	>3.0	<0.094	0.031
1737−30	1740-3015	358.3	+0.2	6	606.7	153	3.3	<5.5	>0.027	0.047
1742−30	1745-3040	358.6	−1.0	14	367.4	88	2.1	<5.5	>0.016	0.042
1821−19	1824-1945	12.3	−3.1	9	189.3	224	5.2	>2.0	<0.112	0.043

density obtained using the Taylor & Cordes (1993) model. The limits derived are fairly wide except for PSR 0906 – 49. It is difficult to derive better distance limits because of the ambiguity arising from the double-valued velocity–distance relationship in these directions, and the lack of accurate kinematic models of the inner Galaxy for purposes of distance determination. The average electron densities derived by us in various directions agree well with those from the model of Taylor & Cordes (1993).

ACKNOWLEDGMENTS

We thank V. Radhakrishnan and G. Srinivasan for critical comments on the manuscript and many useful suggestions. We would also like to thank A. G. Lyne, the referee, for his critical comments, in particular for his suggestions which prompted us to clarify the significance levels for the observed absorption features.

REFERENCES

Altenhoff W. J., Downes D., Goad L., Maxwell A., Rinehart R., 1970, A&AS, 1, 319
Clifton T. R., Lyne A. G., McKenna J., Ashworth M., 1992, MNRAS, 254, 177
Costa M. E., McCulloch P. M., Hamilton P. A., 1991, MNRAS, 252, 13
D'Amico N., Manchester R. N., Durdin J. M., Stokes G. H., Stinerbring D. R., Taylor J. H., Brissenden R. J. V., 1988, MNRAS, 234, 437
Deshpande A. A., McCulloch P. M., Radhakrishnan V., Ananthar-amaiah K. R., 1992, MNRAS, 258, 19P
Dickey J. M., Kulkarni S. R., van Gorkom J. H., Heiles C. E., 1983, ApJS, 53, 529
Fich M., Blitz L., Stark A. A., 1989, ApJ, 342, 272
Frail D., Weisberg J. M., 1990, AJ, 100, 743
Hamilton P. A., Lyne A. G., 1988, MNRAS, 224, 1073
Johnston S., Lyne A. G., Manchester R. N., Kniffen D. A., D'Amico N., Lim J., Ashworth M., 1992, MNRAS, 255, 401
Kerr F. J., Vallak R., 1967, Aust. J. Phys., Astrophysical Supplement Number 3
Koribalski B., Johnston S., Weisberg J. M., Wilson W., 1995, ApJ, 441, 756
Lorimer D. R., Yates J. A., Lyne A. G., Gould M., 1995, MNRAS, 273, 411
Mathewson D. S., Healy J. S., Rome J. M., 1962, Aust. J. Phys., 115, 354
Newton L. M., Manchester R. N., Cooke D. J., 1981, MNRAS, 194, 841
Payne H. E., Salpeter E. E., Terzian Y., 1983, ApJ, 272, 540
Radhakrishnan V., Goss W. M., Murray J. D., Brooks J. W., 1972, ApJS, 241, 1
Siegman B. C., Manchester R. N., Durdin J. M., 1993, MNRAS, 262, 449
Sinclair M. M., Kerr F. J., 1971, Aust. J. Phys., 24, 769
Taylor J. H., Cordes J. M., 1993, ApJ, 411, 674
Wu X., Manchester R. N., Lyne A. G., Qiao G., 1993, MNRAS, 261, 630